Improving Carrier Lifetime of Tin Sulfide *via* Prediction and Mitigation of Harmful Point Defects

Alex Polizzotti[1], Alireza Faghaninia[2], Jeremy R. Poindexter[1], Lea Nienhaus[1], Vera Steinmann[1], Robert L.Z. Hoye[1§], Alexandre Felten[3], Amjad Deyine[4], Niall Mangan[1], Juan Pablo Correa-Baena[1], Seong Sik Shin[1], Shaffiq Jaffer[5], Moungi Bawendi[1], Cynthia Lo[2], Tonio Buonassisi[1]*

[1]Massachusetts Institute of Technology, 77 Massachusetts Avenue, Cambridge, MA 02139, USA

[2]Washington University in St. Louis, 1 Brookings Drive, St. Louis, MO 63130, USA

[3]Université de Namur, Rue de Bruxelles 61, B-5000 Namur, Belgium

[4]TOTAL Solar Research and Development Dpt, 2 place Jean Millier – La Défense 6, 92078 Paris La Défense Cedex, USA

[5]TOTAL American Services, Inc., 82 South St., Hopkington, MA 01748, USA

*****E-mail: a_zotti@mit.edu

*Mailing address: Stata shipping center, 32 Vassar Street, Room 35-211, Cambridge, MA 02139

1[§]Current address: Cavendish Laboratory, University of Cambridge, JJ Thomson Ave, CB3 0HE, UK

Tin monosulfide (SnS) is an emerging thin-film absorber material for photovoltaics. An outstanding challenge is to improve carrier lifetimes to >1 ns, which should enable >10% device efficiencies. However, reported results to date have only demonstrated lifetimes at or below 100 ps. In this study, we employ defect modeling to identify the sulfur vacancy and defects from Fe, Co, and Mo as most recombination-active. We attempt to minimize these defects in crystalline samples through high-purity, sulfur-rich growth and experimentally improve lifetimes to >3 ns – thus achieving our 1 ns goal. This framework may prove effective for unlocking the lifetime potential in other emerging thin film materials by rapidly identifying and mitigating lifetime-limiting point defects.

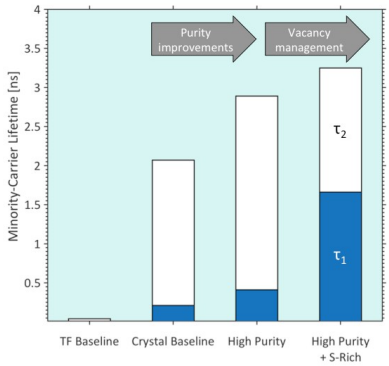

Photovoltaics, thin films, earth-abundant, defects, carrier lifetime

Inorganic thin-film absorbers for photovoltaics (PVs) have struggled to achieve large-scale market penetration; thin film technology constituted less than 7% of 2015 PV energy production[1]. At the same time, technological improvements over current state-of-the-art silicon cells on the market will be necessary to meet cost and climate goals[2,3]. Thin films represent a potential low-cost path to scalable PV. However, the majority of emerging thin film absorbers still underperform in efficiency despite promising optical properties[4], a problem which in many cases can be linked to a short minority-carrier lifetime[5].

Impurity management has been critical to achieving long lifetimes in other materials. Significant improvements in silicon technology were due to understanding the dependence of carrier lifetime on iron[6-10] and other metal impurities[11] that cause deep carrier traps. Certain metal impurities have also been shown to form performance-limiting deep trap states in some thin film semiconductors[12-14].

Controlling vacancies, and intrinsic defects in general, has also proven critical to improving performance, particularly for thin-film PV absorbers. Modeling the complex intrinsic point-defect profiles of $Cu(In,Ga)Se_2$ (CIGS)[15,16] and Cu_2ZnSnS_4 (CZTS)[17,18], for instance, has informed growth parameters to achieve high (>1 ns) lifetimes.

We used tin monosulfide (SnS) as a test case material; while SnS shows promise as an intrinsically *p*-type, earth-abundant and nontoxic material with strong optical properties for PV[19], it is limited by as-of-yet insufficient minority-carrier (electron) lifetimes of <100 ps[5]. Improving electron lifetimes to >1 ns is predicted to enable device efficiency increases from the current record of 4.4%[19] to >10%[20]. Prior work implicates intragranular point defects as limiting carrier transport[21-23].

In this work, we applied a combined modeling and experimental framework to point defect management in SnS, and predict that carrier lifetime depends strongly on the sulfur vacancy defect as well as substitutional defects caused by Fe, Co, and Mo. We independently demonstrate the importance of sulfur content as well as impurity content on lifetime in SnS samples. Moreover, through targeted defect management we achieve – for the first time to our knowledge – SnS minority-carrier lifetimes in excess of 1 ns. This constitutes approximately a two order-of-magnitude increase over previously reported results[5] for thin films, and opens a path to SnS devices with efficiencies >10%. We believe this represents a generalizable path to managing lifetime-limiting defects in novel absorber materials to accelerate future development.

We used Shockley-Read-Hall (SRH) statistics[24-26], informed by density function theory (DFT) calculations of defect energetics, to predict the defect-limited lifetime for all possible intrinsic vacancies, substitutionals, and interstitials, as well as extrinsic point defects caused by any impurities known to be in the material feedstock or growth and processing environments. As shown in Figure 1a, V_S, Mo_{Sn}, Fe_{Sn}, and Co_{Sn} were predicted to have over a two order-of-magnitude more severe effect on carrier lifetime at a given concentration compared to other defects calculated herein. Those defects calculated to have a relatively benign effect on carrier lifetime (such as V_{Sn}, Na_{Sn}, and Sb_{Sn}) due to shallow states, as well as defects with extremely high formation energy (such as S_{Sn} or Sn_S) were excluded from Figure 1a. For details on the DFT and SRH calculations, including relevant assumptions, please refer to the methods.

Defect formation energy curves for the four key defects (as well as the benign acceptor V_{Sn}) are shown in Figure 1b. Defect energy levels, corresponding to charge state transitions, are denoted by circles. Trap levels for the calculated defects show reasonable agreement with previous calculations for defects in SnS[27,28], with the exception of the V_{Sn} defect, which is

predicted here to be within the valence band. We see that all four of these key defects show one or more relatively deep trap levels, and are all positively charged in *p*-type material, thus attracting minority carriers (electrons). These findings suggest that increasing the chemical activity of sulfur, and decreasing that of Fe, Co, and Mo, will lead to significant lifetime improvements in SnS.

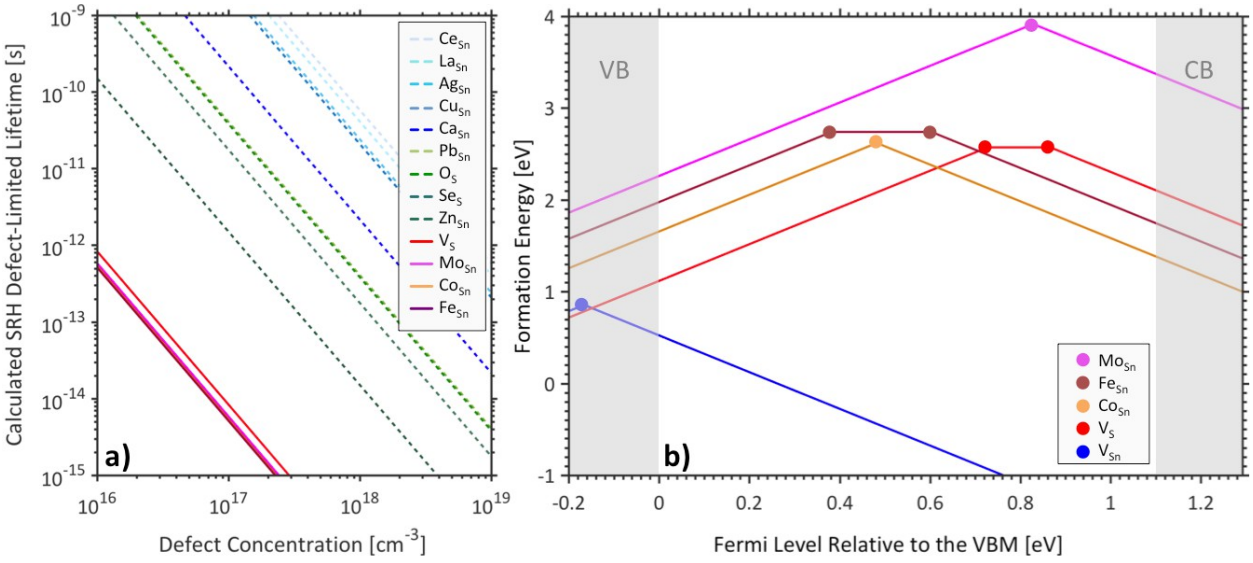

Figure 1. a) Defect-limited lifetimes for likely point defects in SnS. Four defects (intrinsic V_S as well as extrinsic Mo_{Sn}, Fe_{Sn}, and Co_{Sn}, in solid lines) are predicted to be most detrimental to lifetime. **b)** Formation energy vs. Fermi energy for the lowest-energy charge state of these four defects as well as the tin vacancy (V_{Sn}), which acts as a shallow acceptor. Circles represent transitions in charge state, and thus trap levels of each defect. Calculations were performed under sulfur-rich conditions (μ_S = 0 eV, μ_{Sn} = -1.05 eV).

Consistent with the defect calculations above, we observed lifetime increases as we independently increased sulfur content and feedstock purity in SnS crystal samples. Figure 2a compares samples with constant purity but varying sulfur content, while Figure 2b compares

samples of varying purity with sulfur content kept constant. For all samples we estimated carrier lifetimes by fitting time-resolved photoluminescence (TRPL) measurements with biexponential decay functions. Photoluminescence (PL) spectra (Figure 2c) were analyzed to inform optical filter choices for TRPL measurements; spectra for all samples showed dominant emission at 1.3 and 1.78 eV, in agreement with previous optical transition levels reported in the literature[29-31]. A higher-energy shoulder was also seen just above 2 eV, and was particularly pronounced in the sulfur-poor samples.

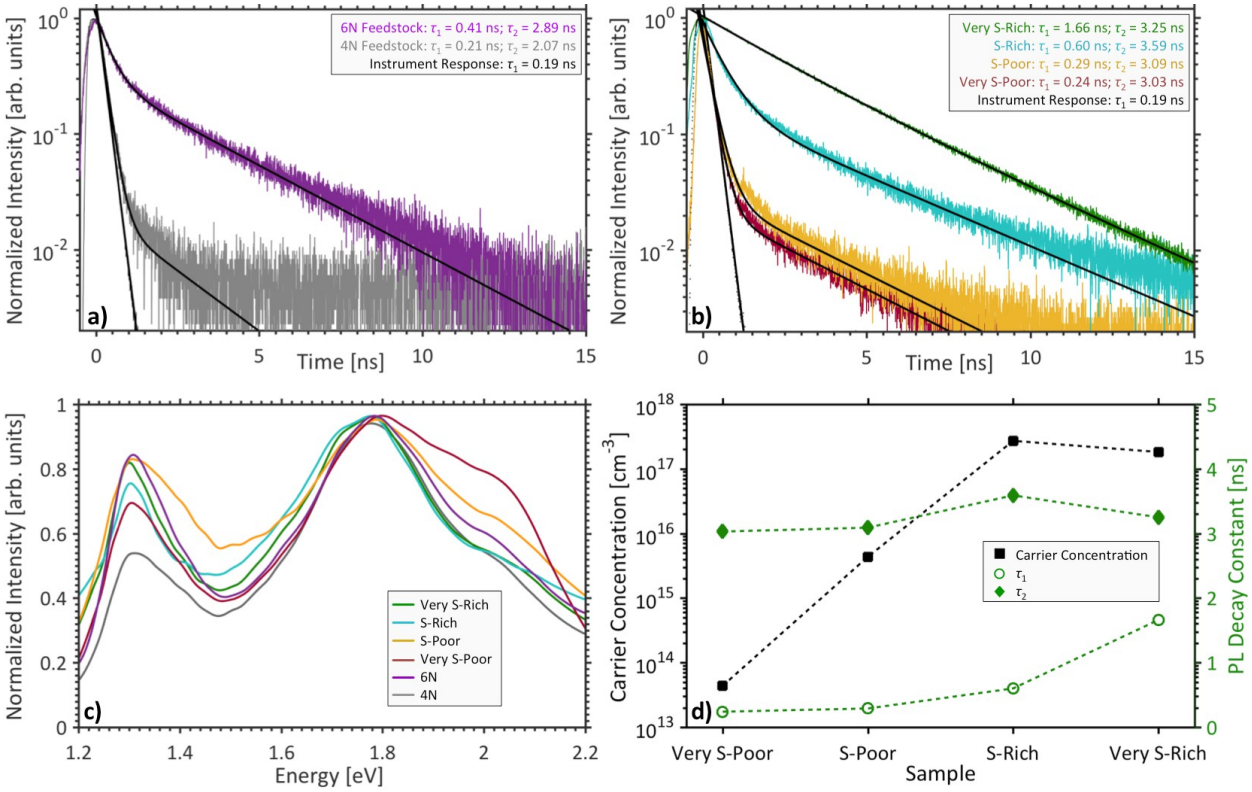

Figure 2. Electro-optical measurements of SnS. **a)** TRPL measurements showing longer decay time constants (and by proxy carrier lifetimes) with increased atomic purity. **b)** TRPL measurements showing that for samples with high atomic purity, increasing sulfur content further lengthens carrier lifetime. **c)** Spectral photoluminescence profiles, showing dominant peaks at

1.3 and 1.78 eV. **d)** Lifetime improvements with increasing sulfur content correlate with an increase in carrier concentration, which can be linked to lower sulfur vacancy concentration.

We observed lifetime increases as we increased purity and sulfur content. Moving from 99.99%-pure (4N) to 99.9999%-pure (6N) feedstock (with over two-order-of-magnitude decreases in key metal content) generated an increase in the fast biexponential decay time constant τ_1 from at or below the instrument response function (IRF) to over 400 ps, as well as a nearly 50% increase in the slower decay constant τ_2. The 4N sample showed the shortest decay constants of all samples (even the sulfur-poor samples, which were grown from higher-purity feedstock). This suggests that adequate purity standards (for SnS, this means Fe, Co, and Mo concentrations in the ppb range or lower) are a prerequisite to achieving long carrier lifetimes in SnS.

In samples made from 6N Sn and 5.5N S, increasing the sulfur-to-tin ratio led to further increases in τ_1 from near the instrument response function to over 1.6 ns. Note that while the Very S-Rich sample has biexponential character, the fit is dominated by the long decay and appears nearly monoexponential. τ_2 increased slightly but is high (>3 ns) for all samples. In agreement with our defect modeling, the highest-performing sample was the Very S-Rich sample, which had the highest sulfur content during growth and was made from high-purity (6N Sn and 5.5N S) feedstocks.

It is as yet unclear why all samples exhibit quite long (>2 ns) values of τ_2 but show large differences in τ_1. In polycrystalline thin films as well as single crystals[32], short- and long-time components of TRPL data have been attributed to surface and bulk lifetimes, respectively. Stoichiometry can affect surface quality, and cation vacancy segregation to surfaces during

growth is thought to have a large effect in polycrystalline CIGS[33]. However, such a mechanism is unlikely in this instance because we exfoliate a surface layer of each sample prior to measurement to expose bulk material. Further work – potentially employing depth-resolved TRPL – is needed to better understand the different recombination pathways in our material.

In order to correlate the improvements in lifetime shown above with reductions in defect density, it is critical to understand relative sulfur vacancy (as well as impurity) concentrations in the SnS samples. We estimate sulfur vacancy content using carrier concentrations extracted from Hall Effect measurements. We assume identical thermal treatment for all samples, low concentrations of extrinsic dopants (as evidenced from impurity measurements, discussed below) and intrinsic interstitial and antisite defects (as evidenced by DFT calculations). Then, in accordance with Kröger-Vink defect chemistry theory[34] for a II-VI binary semiconductor, we can say that the carrier concentration p and the sulfur vacancy content $[V_S]$ are inversely related. As shown in Figure 2d, we observe a nearly 4 order-of-magnitude increase in p between the Very S-Poor and Very S-rich growth conditions, suggesting a commensurate reduction in $[V_S]$. Note that we see a plateau in carrier concentration between the S-Rich and Very S-Rich samples, possibly due to the formation of sulfurous phase impurities at the surface, which would pin the sulfur chemical potential during growth and result in similar V_{Sn} (and thus hole) concentrations in both samples.

The increase in PL decay constants with increasing sulfur content correlated with carrier concentration increases (Fig. 2d), which we associate with decreases in $[V_S]$. Based on our defect calculations in Figure 1a, we expect a two order-of-magnitude change in defect-limited electron lifetimes for every one order-of-magnitude change in $[V_S]$. We do not see such a drastic increase in either decay constant, though τ_1 improved by approximately one order of magnitude between

the “Very S-poor” and “Very S-rich” samples. τ_2 increased slightly as well. This suggests that under these growth conditions, recombination may not be completely dominated by V_S. However, the ability to increase carrier lifetime to well over 1 ns in SnS by altering sulfur and metal impurity content provides us with powerful handles with which to optimize SnS material quality.

To better understand changes in impurity-related defect concentrations, we monitor concentrations of Fe, Mo, and Co — predicted to have the largest impact on carrier lifetime in SnS — using time-of-flight secondary ion mass spectrometry (ToF-SIMS). All samples showed these metals near or below the detection limit, and thus we can only say that these metals are likely at or below several ppm in all samples. We also detect low concentrations of alkali metals and other common dopants, suggesting that our Hall measurements above are likely dominated by intrinsic defects. For further intuition on relative impurity levels, we refer to the feedstock impurity analysis performed by the manufacturer presented in Table 1. For complete SIMS datasets for all samples, see S.I.

Table 1. Atomic concentrations (in ppb) of Fe, Co, and Mo for all feedstocks used in this study.

Feedstock	**6N-pure Sn**	**5.5N-pure S**	**4N-pure SnS**
Supplier	Alfa Aesar	Alfa Aesar	Sigma Aldrich
Measurement	GDMS	GDMS	ICP-MS
Co	<1	50	1000
Fe	<1	<1	3600
Mo	<1	<1	<1

To ensure that all measurements were performed on phase-pure SnS, we performed X-ray diffraction (XRD) and Raman spectroscopy measurements. XRD patterns (Figure 3a) confirmed that the crystallite interior for all samples was phase-pure SnS, with all detected peaks matching literature XRD patterns for orthorhombic SnS (space group *Pnma*).

Raman spectroscopy (Figure 3b) performed on the crystal surfaces and in the bulk revealed that in some of the samples, particularly the sulfur-rich ones, phase impurities were present at the surface of the crystals. However, once a surface layer was exfoliated (thus exposing a pristine interior layer) no further phase impurities were detected.

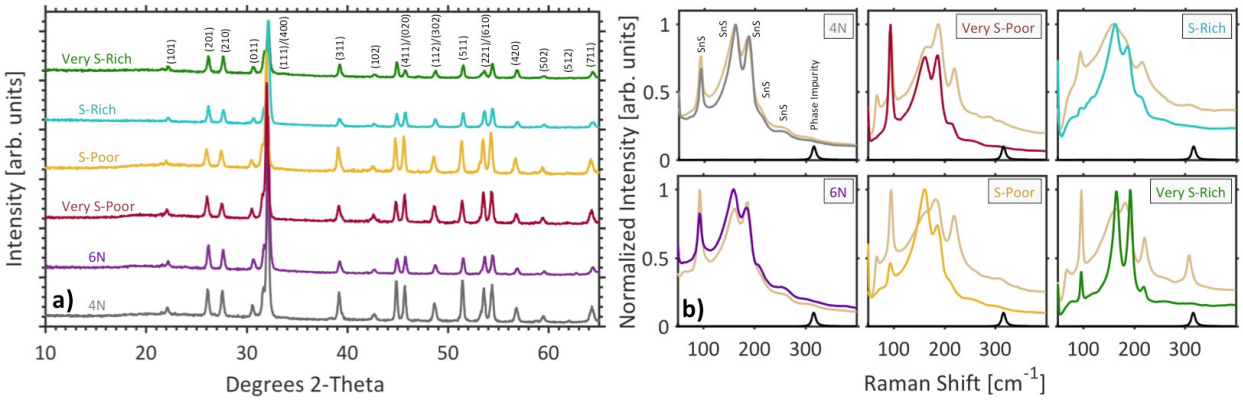

Figure 3. Structural characterization of crystal samples. **a)** XRD patterns indicate phase-pure SnS for all samples. **b)** Raman spectroscopy performed on crystal surfaces (beige curves) showed phase impurities (peak at ~310 cm^{-1}, indicated by black curve) for some samples, which was no longer evident after exfoliation and removal of the surface layer (color-coded curves).

To understand the potential impact of our observed carrier lifetime improvements on devices, we perform SCAPS-1D[35] device simulations to predict device efficiencies assuming realistic device architecture[36] and accounting for parasitic absorption losses. Figure 4 shows calculated iso-efficiency contours as a function of the SnS absorber layer's minority-carrier lifetime and majority carrier concentration. Experimental values are overlaid for previously

reported thin films[5] as well as the 4N and Very S-Rich samples. We predict that the material quality achieved for the Very S-Rich sample is sufficient to achieve >10% efficient devices. For more information regarding device calculations refer to the methods.

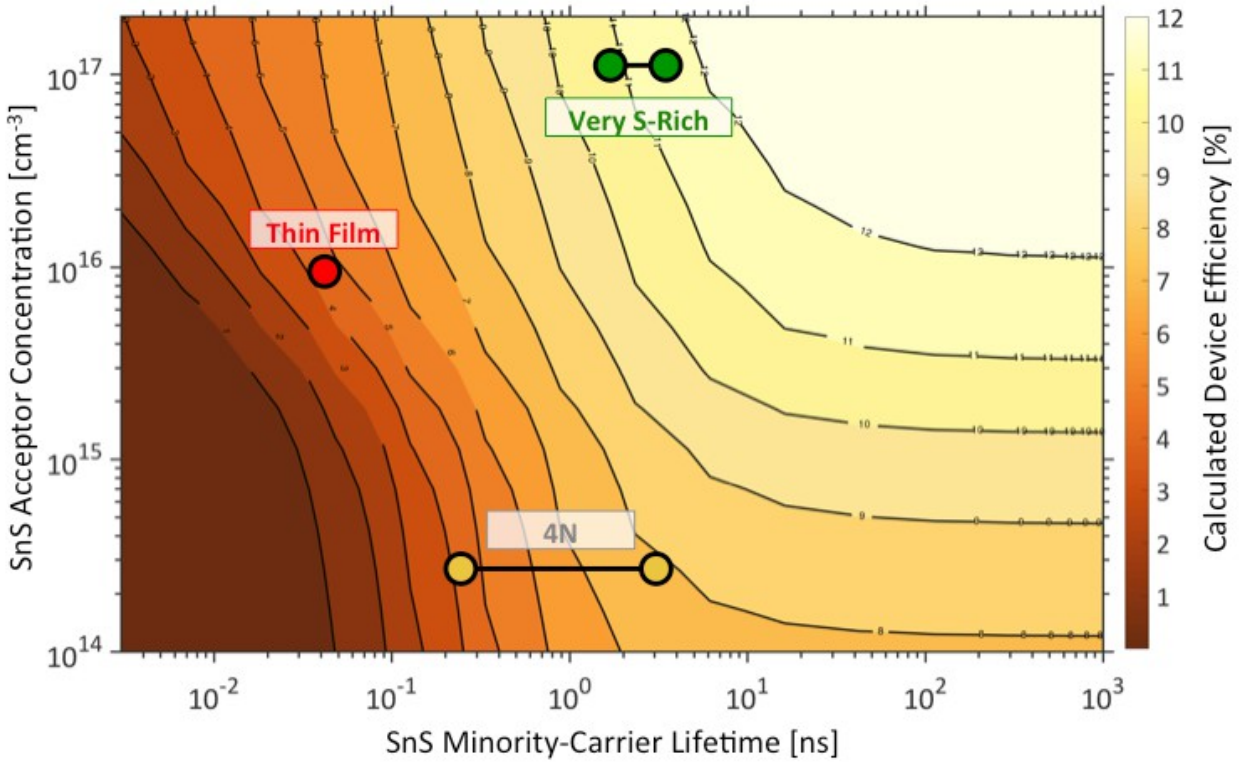

Figure 4. Contour plot of SCAPS-1D device simulations relating efficiency of a realistic SnS device to the SnS minority-carrier lifetime and majority carrier concentration. Experimental data from previously reported thin films as well as the 4N and Very S-Rich samples are overlaid. For the latter two samples, values of τ_1 and τ_2 are both presented.

Several of the methods applied here to SnS should be generalizable to other thin-film materials. Using defect modeling to identify minimum purity requirements and optimal growth stoichiometry can help minimize harmful intrinsic and extrinsic point defects. Primary focus should be placed on impurities known to be present in the material feedstock (certificates of analysis are typically available upon purchase for any commercial feedstock), as well as all

processing equipment. High-purity feedstocks can either be purchased or, in the case of molecular materials, synthesized in lab *via* reaction of high-purity elemental precursors in a high-purity environment. As well, anion overpressure is often a best-practice for chalcogenide materials systems[37].

In this study we significantly improved carrier lifetime in SnS through defect management guided by theoretical predictions. Moreover, we demonstrated the ability to span the range from *a priori* defect calculations to experimental lifetime improvements in an emerging thin-film material.

In conclusion, we predicted that four defects are particularly detrimental to carrier lifetime in SnS – the intrinsic vacancy V_S and the extrinsic substitutionals Co_{Sn}, Fe_{Sn}, and Mo_{Sn}. Separately, we demonstrated experimentally that both increasing sulfur content and reducing impurity concentration result in significant improvements in minority-carrier lifetime. Our device simulations suggest that these observed long lifetimes, when achieved in thin-film form, may enable SnS devices with efficiencies >10%. Moreover, we hope that a similar approach can accelerate improvements in other emerging materials.

Vienna ab initio Simulation Package[38,39] was used for density functional theory (DFT) defect calculations with the exchange-correlation functional of Perdew-Burke-Ernzerhof[40], generalized gradient approximation, and projector augmented-wave (PAW)[41,42] pseudopotentials. Additionally the Heyd-Scuseria-Ernzerhof hybrid functional[43,44] was employed with an exchange coefficient of 0.1 to accurately calculate the indirect band gap of 1.1 eV for SnS[45]. For defect calculations, we use a 72-atom supercell (3x3x3) with a 2x2x2 grid of k-points. Calculations account for spin polarization, but not spin orbit coupling due to calculation cost. Calculations

were performed assuming a sulfur-rich environment, with the chemical potential of sulfur set to zero, and that of Sn at -1.05 eV (the formation enthalpy of SnS). Note that going to S-poor conditions would exhibit a shift in formation energy (specifically, a decrease for V_S and increase for V_{Sn}) but not in trap levels. For more detail regarding the defects calculation methodology and assumptions regarding chemical potentials, as well as prior examples of similar calculations, see references[46-48].

Vacancies as well as all impurities known to be in the SnS, Sn, or S feedstocks, or in any materials used during processing such as the quartz amouples, were included in calculations. Intrinsic antisites and interstitials were found to have very high formation energy from DFT and were excluded from SRH calculations.

The calculated defect charge transition levels were input into an SRH statistical model to calculate defect-limited lifetime (i.e. the material lifetime assuming recombination *only* through a given defect) as a function of that defect's concentration according to the relations laid out in[24]. Capture cross-sections were estimated assuming a purely Coulombic model, which has been shown to approximate capture cross sections in established materials to within an order of magnitude[49]. Multivalent states were simplified into multiple single-level SRH-like defects according to established guidelines[50]. Material parameters are estimated based on prior literature – hole concentration of 10^{16} cm^{-3} [23] with an assumed 10% compensation, relative permittivity of 37.3[51], and effective masses $m_h = 3m_e = 1.5m_o$[28]. Because of the assumptions stated above, results should be treated as qualitative.

Device simulations were performed using SCAPS-1D software[35], the results of which were batched and analyzed in MATLAB to produce contour plots of device efficiency vs. absorber layer minority-carrier lifetime and majority-carrier concentration. Material and device

parameters for a “present day” device, including realistic parasitic absorption losses, can be found in[36].

Two sets of SnS crystal samples were grown from the melt to separately evaluate the effects of sulfur content as well as impurity content.

For the first set, crystals were grown using molecular SnS feedstock at two different impurity levels—99.99% (4N) and 99.9999% (6N). 4N SnS was obtained from Sigma Aldrich. 6N SnS, not available commercially, was synthesized in-house from 6N-pure Sn from Alfa Aesar and 4% H_2S gas in N_2 balance with negligible metal content by heating Sn in a tube furnace for several hours at 600°C with 100 sccm H_2S flow.

For the second set, sulfur content was varied. All crystals were synthesized from elemental 6N-pure Sn and 5.5N-pure S, both from Alfa Aesar. Crystals were grown with Sn/S ratios of 48/52 (“Very Sulfur-Rich”), 49/51 (“Sulfur-Rich”), 51/49 (“Sulfur-Poor”), and 52/48 (“Very Sulfur-Poor”).

Regardless of feedstock, all crystals were grown in ampoules of 4.5N-pure quartz sealed under 2 Torr of Ar, heated to 950°C over 2 hours, held at 950°C for 12 hours, and cooled to room temperature over 5 days at 0.125°C/min.

Samples were cut from crystals and mounted with the basal (100) plane parallel to glass substrates. SnS has a layered orthorhombic structure, and it is possible to exfoliate layers along the (100) plane using tape. Unless otherwise stated, all samples were exfoliated in this way before measurements were performed. This exposes a pristine layer within the crystal bulk and ensures that all measurements are performed on phase-pure SnS.

Spectral photoluminescence (PL) and Raman spectroscopy measurements were both performed under ambient conditions on a Horiba LabRam multiline Raman/PL

Spectrophotometer using a 532 nm laser operating at 2 mW, focused on a ~500 nm diameter Gaussian spot with a 50x confocal microscope objective. Total exposure time was ~30 s (Raman) and ~15 min (PL). Samples were visually inspected before and after measurements and repeat measurements were performed at the same location to ensure repeatability.

X-ray diffraction (XRD) was performed on a Bruker D8 X-ray diffractometer with a General Area Detector Diffraction System employing Cu Kα radiation. Samples were prepared as powders according to best practices[52].

Time-of-flight secondary ion mass spectrometry (ToF-SIMS) impurity analysis was performed on an ION ToF-SIMS 4 using Bi_1^+ as primary ions. Profiles were performed using 2 keV O_2 (positive polarity) and Cs (negative polarity) primary ions.

Lifetime data was collected under ambient conditions without background illumination using a time-correlated single photon counting (TCSPC) system using a PicoQuant LDH-P-FA530B 532 nm picosecond laser. Samples were illuminated under 50±1 μW illumination on a ~180-μm-diameter spot with a 10 MHz repetition rate, corresponding to a fluence of ~4.9 nJ/(cm^2□pulse). PL emission was collected using a Micro Photon Devices, $PD-100-C0C single-photon-sensitive avalanche photodiode. The collected radiation was filtered through a 532 nm notch filter, 800 nm short pass filter, and 550 nm longpass filter.

Hall Effect measurements were performed using a Keithley 4200 semiconductor characterization system. Samples were prepared in the Van der Pauw configuration[53] with 200-nm-thick 0.1x0.1mm gold contacts on top of a 20 nm Ti adhesion layer. Data was taken under magnetic fields between ±1.5 Tesla in 0.1 T increments.

The authors declare no competing financial interest.

Supporting Information: Additional DFT defect and band structure / density-of-states calculations for SnS, SIMS scans for all samples, X-ray photoemission spectroscopy analysis of Sn chemical state in all samples

The authors give particular thanks to Katy Hartman, whose research on tuning intrinsic defects in SnS thin films inspired this work. We also thank Rupak Chakraborty and Roy Gordon for helpful conversations, as well as Jim Serdy for advice on ampoule sealing and a plethora of other topics. This work was supported in part under the U.S.-India Partnership to Advance Clean Energy- Research for the Solar Energy Research Institute for India and the United States, funded jointly by the U.S. Department of Energy (Office of Science, Office of Basic Energy Sciences, and Energy Efficiency and Renewable Energy, Solar Energy Technology Program, under Subcontract DE-AC36-08GO28308 to the National Renewable Energy Laboratory, Golden, CO, USA) and the Government of India through the Department of Science and Technology under Subcontract IUSSTF/JCERDC-SERIIUS/2012 dated November 22, 2012. A. Polizzotti acknowledges an NSF Graduate Research Fellowship. Work by V. Steinmann and N. Mangan was funded by the U.S. Department of Energy through the SunShot Initiative under Contract No. DE-EE0005329. Work by J.R. Poindexter, R.L.Z. Hoye, J.P. Correa-Baena, and S.S. Shin was supported by a TOTAL SA research grant funded through MIT*ei*. L. Nienhaus was supported as part of the Center for Excitonics, an Energy Frontier Research Center funded by the US Department of Energy, Office of Science, Office of Basic Energy Sciences under Award Number DE-SC0001088 (MIT). This work used the Center for Materials Science and Engineering at

MIT, which is supported by NSF award DMR-08-19762, and the Center for Nanoscale Systems at Harvard University under NSF award ECS-0335765.

(1) *Photovoltaics Report*; Technical Report for Fraunhofer Institute for Solar Energy Systems with Support of PSE AG: Freiburg, November 2016.

(2) Kurtz, S.; Atwater, H.; Rockett, A.; Buonassisi, T.; Honsberg, C.; Benner, J. Solar Research not Finished. *Nat. Photonics* **2016**, *10*, 141–142.

(3) Needleman, D. B.; Poindexter, J.R.; Kurchin, R.C.; Peters, I.M.; Wilson, G.; Buonassisi, T. Economically Sustainable Scaling of Photovoltaics to Meet Climate Targets. *Energy Environ. Sci.* **2016**, *9*, 2122–2129.

(4) Steinmann, V.; Brandt, R. E.; Buonassisi, T. Photovoltaics: Non-Cubic Solar Cell Materials. *Nat. Photonics* **2015**, *9*, 355–357.

(5) Jaramillo, R.; Sher, M.-J.; Ofori-Okai, B.K.; Steinmann, V.; Yang, C.; Hartman, K.; Nelson, K.A.; Lindenberg, A.M.; Gordon, R.G.; Buonassisi, T. Transient Terahertz Photoconductivity Measurements of Minority-Carrier Lifetime in Tin Sulfide Thin Films: Advanced Metrology for an Early Stage Photovoltaic Material. *J. Appl. Phys.* **2016**, *119*, 035101.

(6) Wong-Leung, J.; Eaglesham, D.J.; Sapjeta, J.; Jacobson, D.C.; Poate, J.M.; Williams, J.S. The Precipitation of Fe at the Si–SiO2 Interface. *J. Appl. Phys.* **1998**, *83*, 580–584.

(7) Istratov, A. A.; Buonassisi, T.; McDonald, R.J.; Smith, A.R.; Schindler, R.; Rand, J.A.; Kalejs, J.P.; Weber, E.R. Metal Content of Multicrystalline Silicon for Solar Cells and its Impact on Minority Carrier Diffusion Length. *J. Appl. Phys.* **2003**, *94*, 6552.

(8) Istratov, A. A.; Hieslmair, H.; Weber, E. R. Iron Contamination in Silicon Technology. *Appl. Phys. A* **2000**, *70*, 489–534.

(9) Hofstetter, J.; Fenning, D.P.; Bertoni, M.I.; Lelièvre, J.F. Impurity-to-Efficiency Simulator: Predictive Simulation of Silicon Solar Cell Performance Based on Iron Content and Distribution. *Prog. Photovolt. Res. Appl.* **2011**, *19*, 487–497.

(10) Powell, D. M.; Fenning, D.P.; Conrad, B.S.; Hofstetter, J.; Lelièvre, J.F.; del Cañizo, C.; Buonassisi, T. Deployment of Impurity-to-Efficiency (I2E) Simulation Tool. *2011 37th IEEE Photovoltaic Specialists Conference* **2011**, 001124–001126.

(11) Davis, J. Jr.; Rohatgi, A.; Hopkins, R.H.; Blais, P.D.; Rai-Choudhury, P.; McCormick, J.R.; Mollenkopf, H.C. Impurities in Silicon Solar Cells. *IEEE Trans. Electron Devices* **1980**, *27*, 677–687.

(12) Collord, A. D.; Xin, H.; Hillhouse, H. W. Combinatorial Exploration of the Effects of Intrinsic and Extrinsic Defects in $Cu_2ZnSn(S,Se)_4$. *IEEE J. Photovolt.* **2015**, *5*, 288–298.

(13) van Leest, R. H.; Bauhuis, G.J.; Mulder, P.; van der Heijden, R.; Bongers, E.; Vlieg, E.; Schermer, J.J. Effects of Copper Diffusion in Gallium Arsenide Solar Cells for Space Applications. *Sol. Energy Mater. Sol. Cells* **2015**, *140*, 45–53.

(14) Balcioglu, A.; Ahrenkiel, R. K.; Hasoon, F. Deep-Level Impurities in CdTe/CdS Thin-Film Solar Cells. *J. Appl. Phys.* **2000**, *88*, 7175–7178.

(15) Repins, I.; Contreras, M.A.; Egaas, B.; DeHart, C.; Scharf, J.; Perkins, C.L.; To, B.; Noufi, R. 19.9%-Efficient ZnO/CdS/$CuInGaSe_2$ Solar Cell with 81.2% Fill Factor. *Prog. Photovolt. Res. Appl.* **2008**, *16*, 235–239.

(16) Wei, S.-H.; Zhang, S. B. Defect Properties of $CuInSe_2$ and $CuGaSe_2$. *J. Phys. Chem. Solids* **2005**, *66*, 1994–1999.

(17) Chen, S.; Walsh, A.; Gong, X.-G.; Wei, S.-H. Classification of Lattice Defects in the Kesterite Cu_2ZnSnS_4 and $Cu_2ZnSnSe_4$ Earth-Abundant Solar Cell Absorbers. *Adv. Mater.* **2013**, *25*, 1522–1539.

(18) Chen, S.; Gong, X. G.; Walsh, A.; Wei, S.-H. Defect Physics of the Kesterite Thin-Film Solar Cell Absorber Cu_2ZnSnS_4. *Appl. Phys. Lett.* **2010**, *96*, 021902.

(19) Sinsermsuksakul, P.; Hartman, K.; Kim, S.B.; Heo, J.; Sun, L. Overcoming Efficiency Limitations of SnS-Based Solar Cells. *Adv. Energy Mater.* **2014**, *4*, 053901.

(20) Mangan, N. M.; Brandt, R.E.; Steinmann, V.; Jaramillo, R.; Li, J.V.; Poindexter, J.R.; Hartman, K.; Sun, L.; Gordon, R.G.; Buonassisi, T. A Path to 10% Efficiency for Tin Sulfide Devices. *Photovoltaic Specialist Conference (PVSC), 2014 IEEE 40th* **2014**, 2373–2378.

(21) Chakraborty, R. Structural Defect Engineering of Tin (II) Sulfide Thin Films for Photovoltaics. PhD Thesis, Massachusetts Institute of Technology, June 2016.

(22) Steinmann, V.; Jaramillo, R; Hartman, K.; Chakraborty, R.; Brandt, R.E.; Poindexter, J.R.; Lee, Y.S.; Sun, L.; Polizzotti, A.; Park, H.H.; Gordon, R.G.; Buonassisi, T. 3.88% Efficient Tin Sulfide Solar Cells Using Congruent Thermal Evaporation. *Adv. Mater.* **2014**, *26*, 7488-7492.

(23) Hartman, K. Annealing for Intrinsic Point-Defect Control and Enhanced Solar Cell Performance: The Case of H_2S and Tin Sulfide (SnS). PhD Thesis, Massachusetts Institute of Technology, February 2015.

(24) Shockley, W.; Read Jr., W. T. Statistics of the Recombinations of Holes and Electrons. *Phys. Rev.* **1952**, *87*, 835.

(25) Hall, R.N. Electron-Hole Recombination in Germanium. *Phys. Rev.* **1952**, *87*, 387.

(26) Sah, C.-T.; Noyce, R.; Shockley, W. Carrier Generation and Recombination in pn Junctions and pn Junction Characteristics. *Proc. IRE* **1957**, *45*, 1228–1243.

(27) Malone, B. D.; Gali, A.; Kaxiras, E. First Principles Study of Point Defects in SnS. *Phys Chem Chem Phys* **2014**, *16*, 26176–26183.

(28) Vidal, J.; Lany, S.; d'Avezac, M.; Zunger, A.; Zakutayev, A.; Francis, J.; Tate, J. Band-Structure, Optical Properties, and Defect Physics of the Photovoltaic Semiconductor SnS. *Appl. Phys. Lett.* **2012**, *100*, 032104.

(29) Devika, M.; Reddy, N.K.; Prashantha, M.; Ramesh, K.; Reddy, S.V.; Hahn, Y.B.; Gunasekhar, K.R. The Physical Properties of SnS Films Grown on Lattice-Matched and Amorphous Substrates. *Phys. Status Solidi A* **2010**, *207*, 1864–1869.

(30) Reddy, R.K.T.; Reddy, N.K.; Miles, R.W. Photovoltaic Properties of SnS Based Solar Cells. *Sol. Energy Mater. Sol. Cells* **2006**, *90*, 3041–3046.

(31) Sorgenfrei, T.; Hofherr, F.; Jauß, T.; Cröll, A. Synthesis and Single Crystal Growth of SnS by the Bridgman-Stockbarger Technique. *Cryst. Res. Technol.* **2013**, *48*, 193–199.

(32) Barnard, E. S.; Hoke, E.T.; Connor, S.T.; Groves, J.R.; Kuykendall, T.; Yan, Z.; Samulon, E.C.; Bourret-Courchesne, E.D.; Aloni, S.; Schuck, P.J.; Peters, C.H.; Hardin, B.E. Probing Carrier Lifetimes in Photovoltaic Materials using Subsurface Two-Photon Microscopy. *Sci. Rep.* **2013**, *3*, 2089.

(33) Yan, Y.; Jiang, C.-S.; Noufi, R.; Wei, S.-H.; Moutinho, H.R.; Al-Jassim, M.M. Electrically Benign Behavior of Grain Boundaries in Polycrystalline $CuInSe_2$ Films. *Phys. Rev. Lett.* **2007**, *99*, 235504.

(34) Kröger, F. A.; Vink, H. J. Relations Between the Concentrations of Imperfections in Solids. *J. Phys. Chem. Solids* **1958**, *5*, 208–223.

(35) Burgelman, M.; Verschraegen, J.; Degrave, S.; Nollet, P. Modeling Thin-Film PV Devices. *Prog. Photovolt. Res. Appl.* **2004**, *12*, 143–153.

(36) Mangan, N. M.; Brandt, R.E.; Steinmann, V.; Jaramillo, R.; Yang, C.; Poindexter, J.R.; Chakraborty, R.; Park, H.H.; Zhao, X.; Gordon, R.G.; Buonassisi, T. Framework to Predict Optimal Buffer Layer Pairing for Thin Film Solar Cell Absorbers: A Case Study for Tin Sulfide/Zinc Oxysulfide. *J. Appl. Phys.* **2015**, *118*, 115102.

(37) Repins, I.; Vora, N.; Beall, C.; Wei, S.-H.; Yan, Y.; Romero, M.; Teeter, G.; Du, H.; To, B.; Young, M.; Noufi, R. Kesterites and Chalcopyrites: A Comparison of Close Cousins. *MRS Proceedings* **2011**, *1324*, 97-108.

(38) Kresse, G.; Furthmüller, J. Efficient Iterative Schemes for Ab Initio Total-Energy Calculations Using a Plane-Wave Basis Set. *Phys. Rev. B* **1996**, *54*, 11169–11186.

(39) Kresse, G.; Furthmüller, J. Efficiency of Ab-Initio Total Energy Calculations for Metals and Semiconductors Using a Plane-Wave Basis Set. *Comput. Mater. Sci.* **1996**, *6*, 15–50.

(40) Perdew, J. P.; Burke, K.; Ernzerhof, M. Generalized Gradient Approximation Made Simple. *Phys. Rev. Lett.* **1996**, *77*, 3865–3868.

(41) Blöchl, P. E. Projector Augmented-Wave Method. *Phys. Rev. B* **1994**, *50*, 17953–17979.

(42) Kresse, G.; Joubert, D. From Ultrasoft Pseudopotentials to the Projector Augmented-Wave Method. *Phys. Rev. B* **1999**, *59*, 1758–1775.

(43) Heyd, J.; Scuseria, G. E.; Ernzerhof, M. Hybrid Functionals Based on a Screened Coulomb Potential. *J. Chem. Phys.* **2003**, *118*, 8207–8215.

(44) Paier, J.; Marsman, M.; Hummer, K.; Kresse, G.; Gerber, I.C.; Ángyán, J.G. Screened Hybrid Density Functionals Applied to Solids. *J. Chem. Phys.* **2006**, *125*, 249901.

(45) Lambros, A.P.; Geraleas, D.; Economou, N.A. Optical Absorption Edge in SnS. *J. Phys. Chem. Solids* **1974**, *35*, 537-541.

(46) Makov, G.; Payne, M. C. Periodic Boundary Conditions in Ab Initio Calculations. *Phys. Rev. B* **1995**, *51*, 4014–4022.

(47) Faghaninia, A.; Lo, C. S. First Principles Study of Defect Formation in Thermoelectric Zinc Antimonide, β-Zn_4Sb_3. *J. Phys. Condens. Matter* **2015**, *27*, 125502.

(48) Freysoldt, C.; Grabowski, B.; Hickel, T.; Neugebauer, J.; Kresse, G.; Janotti, A.; Van de Walle, C.G. First-Principles Calculations for Point Defects in Solids. *Rev. Mod. Phys.* **2014**, *86*, 253–305.

(49) Bube, R. H. *Photoelectronic Properties of Semiconductors*. Cambridge University Press: Cambridge, 1992; pp 105-113.

(50) Decock, K.; Khelifi, S.; Burgelman, M. Can a Multivalent Defect be Mimicked by Several Shockley–Read–Hall-Like Defects? *J. Appl. Phys.* **2010**, *108*, 063707.

(51) Madelung, O. *Semiconductors: Data Handbook (3rd ed.)*. Springer: Berlin Heidelberg, 2004; pp 1981-1989.

(52) Hoye, R. L. Z.; Schulz, P.; Schelhas, L.T.; Holder, A.M.; Stone, K.H.; Perkins, J.D.; Vigil-Fowler, D.; Siol, S.; Scanlon, D.O.; Zakutayev, A.; Walsh, A.; Smith, I.C.; Melot, B.C.; Kurchin, R.C.; Wang, Y.; Shi, J.; Marques, F.C.; Berry, J.J.; Tumas, W.; Lany, S.; Stevanović, V.; Toney, M.F.; Buonassisi, T. Perovskite-Inspired Photovoltaic Materials: Toward Best Practices in Materials Characterization and Calculations. *Chem. Mater.* **2017**, *29*, 1964–1988.

(53) Van der Pauw, L. J. A Method of Measuring the Resistivity and Hall Coefficient on Lamellae of Arbitrary Shape. *Philips Tech. Rev.* **1958**, *26*, 220–224.